Nanoscale

PAPER

View Article Online
View Journal | View Issue

Cite this: *Nanoscale*, 2023, **15**, 14809

Light-gated specific oxidase-like activity of a self-assembled Pt(II) nanozyme for environmental remediation†

Rohit Kapila, Bhaskar Sen, Alisha Kamra, Shana Chandran and Subinoy Rana *

Artificial enzyme equivalents, also known as nanozymes, are a practical tool for environmental remediation when compared to their natural counterparts due to their high operational stability, efficiency, and cost-effectiveness. Specific oxidase mimicking nanozymes are well suited to degrade toxic chemicals from industrial waste such as phenols and azo dyes. Therefore, photocatalytic nanozymes using visible/sunlight would provide a viable strategy for sustainable environmental remediation. Herein, we introduce an aggregation-induced emissive Pt(II) complex, which self-assembles in water providing **NanoPtA** nanotapes. These structures exhibit a specific oxidase-like nanozyme activity driven by light. The **NanoPtA** structure assists in the photogeneration of singlet oxygen in water *via* a triplet excited ^{3}MMLCT state, leading to a specific oxidase-like activity instead of a peroxidase-like activity. The self-assembled nanozyme showed great stability under harsh environmental conditions and exhibited photo-induced specific oxidase-mimetic activity, which was considerably more efficient than the natural enzyme or other specific nanozymes. We demonstrated efficient **NanoPtA**-induced photocatalytic degradation of various phenolic compounds and azo dyes within 5–10 minutes of light irradiation. Notably, the system operates under sunlight and exhibits reusability over twenty cycles of catalytic reactions. Another fascinating aspect of **NanoPtA** is the unaltered catalytic performance for more than 75 days, providing a robust enzyme-equivalent for practical sustainable environmental remediation.

Received 5th May 2023,
Accepted 14th August 2023

DOI: 10.1039/d3nr02081a

rsc.li/nanoscale

1. Introduction

Natural enzymes as biocatalysts are known for their specificity and efficiency in catalyzing biological reactions in living systems.[1] However, they possess certain limitations that hinder their broad applications, including restricted stability, reduced efficacy under harsh conditions, and tedious as well as expensive synthesis and purification procedures. These limitations and their short shelf life impede their practical use and adoption in various industrial sectors.[2,3] To address these challenges, a class of nanomaterials that possess enzyme-equivalent activity, known as nanozymes, has been extensively studied.[4,5] Nanozymes traditionally refer to nanomaterials that facilitate the conversion of enzyme substrates into products, exhibiting reaction kinetics following the Michaelis–Menten model under physiological conditions, irrespective of their working mechanism compared to the natural enzyme.[6] Essentially, nanozymes are artificial synthetic enzymes that display enzyme-like activities. Nanozymes typically consist of catalytically active metal ions and often organic linkers, which contribute to their enzyme mimetic properties. Compared to natural enzymes, nanozymes exhibit superior catalytic performance, selectivity, and stability in various applications including point-of-care diagnostics,[7] biotechnology,[8] antibacterial agents,[9] and biofuel production.[10] Diverse natural enzyme-like catalytic activities have been achieved using nanozymes, such as peroxidase,[11,12] superoxide dismutase,[13,14] esterase,[15,16] oxidase,[17,18] catalase,[19,20] and haloperoxidase.[21,22] A notable feature of nanozymes is the more expansive physical and chemical operational windows, including high salt concentration, temperature, and pH tolerance.[2] Due to the advantages of stability under harsh conditions and superior enzymatic performance over natural enzymes, nanozymes would be excellent candidates for environmental monitoring and remediation in challenging and unpredictable outdoor environments.

The development of nanozymes with multiple enzymatic activities has mainly focused on designing micro/nanostructures using metals/metal oxides,[23,24] carbon-based nano-

Materials Research Centre, Indian Institute of Science, C. V. Raman Road, Bangalore 560012, Karnataka, India. E-mail: subinoy@iisc.ac.in; Tel: +91 080-22932914

† Electronic supplementary information (ESI) available. See DOI: https://doi.org/10.1039/d3nr02081a

materials,[25] polymers,[26,27] and metal–organic frameworks.[28,29] Although these materials have effective enzyme equivalent activities, certain challenges including non-dynamic nature under different stimuli, lack of specificity, low density of active sites, and complex/multi-step synthesis procedures restrict the achievement of "life-like" materials. Using the principles of supramolecular chemistry to mimic enzymes offers great opportunities to achieve such biomimetic materials. This strategy includes the development of nanozymes based on supramolecular structures that share a number of important characteristics similar to natural enzymes such as amphiphilicity, precise control of conformational states, supramolecular interactions driving substrate recognition for augmented activity, and specific hydrophobic microenvironments for catalysis.[30] Supramolecular nanozymes provide modular and adaptive platforms that are created by assembling building blocks using noncovalent interactions,[31] enabling the design of soft-materials to mimic the coordination environment found in enzyme active sites. Significantly, supramolecular nanozymes present essential features in common with natural enzymes. Consequently, diverse supramolecular nanozymes have been introduced containing different scaffolds such as peptides,[32] micelles,[33] vesicles,[34] nanofibers,[35] nanotubes,[36] metal coordinated system,[37] and hydrogels.[38] Metal-based supramolecular systems including metal complexes,[39] metallacycles,[40] and metallacages[41] offer useful spectroscopic properties including aggregation induced emission (AIE), which can be exploited to achieve nanozyme activities. For example, reactive oxidative species (ROS) enable specific oxidase mimetic catalysis,[42] unlike traditional nanozymes, which show mixed peroxidase-like activity. Specific oxidase mimetic enzyme-equivalents avoid hydrogen peroxide in the reaction medium and have great implications in practical applications including therapeutics and environmental remediation.

Self-assembled metallo-supramolecular complexes featuring AIE offer promising platforms for generating photo-regulated reactive oxygen species. These supramolecular systems utilize bottom-up assemblies through the unique noncovalent metal–metal and π–π interactions, with advantageous photophysical properties.[43] Herein, we developed a supramolecular Pt(II)-based nanotape assembly (**NanoPtA**), which causes enhanced AIE in aqueous medium as depicted in Scheme 1. This system shows excellent visible light-driven oxidase mimetic activity, precluding any peroxidase-like activity. Mechanistic studies suggest that the photocatalytic generation of singlet oxygen in the aqueous medium bestows the specific oxidase activity. The enzyme equivalent activity allowed us to explore the potential of **NanoPtA** in degrading organic pollutants and selective azo dye degradation as an environmental remediation approach. The system showed catalytic activity against a range of phenolic and azo-dye substrates. Given the exciting aspect of **NanoPtA** operating under sunlight/visible light, the present nanozyme is poised to demonstrate practical environmental sustainability. In addition, a practical feature of **NanoPtA** is its reusability for at least 20 cycles, retaining its catalytic activity for more than 75 days. To the best of our knowledge this is the first report on light-gated specific oxidase-like activity using the Pt(II) complex assembly. This system presents a highly desirable alternative to conventional oxidation methods that often suffer from selectivity and efficacy.

2. Experimental details

Materials

All the chemicals and solvents used for synthesis and spectroscopic studies were used as received without further purification. Chemicals such as 2,6-pyridinedicarboxylic acid, *o*-phenylenediamine (OPD), polyphosphoric acid (PPA), dopamine hydrochloride, 4-amino antipyrine (4-AP), 2,4-dichlorophenol (2,4-DP), 2,2′-azino-bis(3-ethylbenzo thiazoline-6-sulfonic acid) (ABTS), 3,3′,5,5′-tetramethylbenzidine (TMB), Congo red, Reactive Red 52, methanol and phenols were obtained from SRL chemicals, India. 4-Methoxyphenol, 4-nitrophenol were purchased from Spectrochem, India. Malachite green oxalate, Evans Blue, Amido Black 10B and Amaranth were obtained from Avra chemicals, India. Adrenaline and Sudan Black were purchased from TCI chemicals. Trypan blue and HEPES (N-2-hydroxyethylpiperazine-N'-2-ethanesulfonic acid)

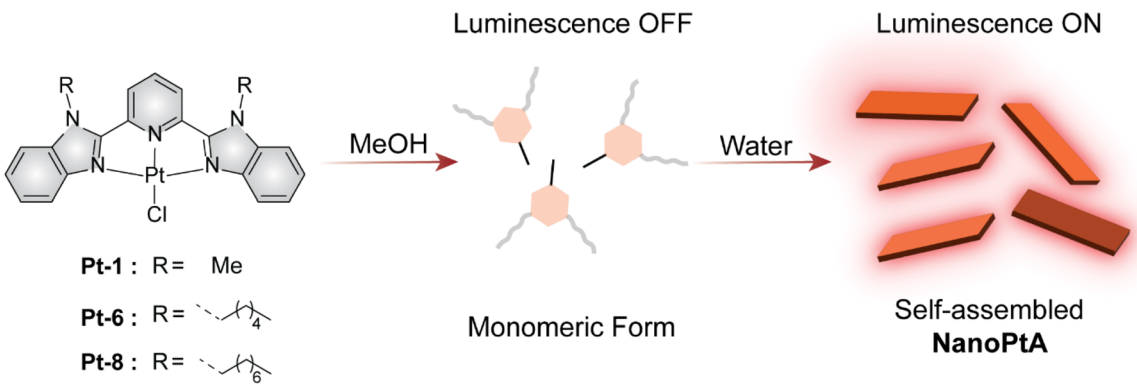

Scheme 1 A schematic illustration of **NanoPtA** assembly formation in water with variation in chain length resulting in different luminescence.

bufferwere obtained from Sigma-Aldrich. All the experiments were performed using Milli-Q water.

Synthesis of the ligands and complexes

Synthesis of 2,6-bis(1*H*-benzo[*d*]imidazol-2-yl)pyridine (BiP). 2,6-Pyridine-dicarboxylic acid (0.50 g, 2.99 mmol), 1,2-diaminobenzene (0.71 g, 6.58 mmol), and 10 mL of polyphosphoric acid (PPA) were placed in a 250 mL round-bottom flask. After that, the reaction mixture was heated at 230 °C under N_2 for 5 h. Then, the green-colored reaction mixture was added to distilled water (350 mL) and the pH was adjusted to 11.0 by adding ammonium hydroxide, which gave a white precipitate. The precipitate was filtered out, thoroughly washed with distilled water, and recrystallized from methanol, which afforded white needle-shaped crystals with a good yield (0.74 g, 80%).

Synthesis of 2,6-bis(1-hexyl-1*H*-benzo[*d*]imidazol-2-yl) pyridine (C_6-BiP). BiP (0.50 g, 1.6 mmol) and NaH (0.19 g, 8.0 mmol) were placed in a 50 mL 2 neck round-bottom flask and degassed under N_2 atmosphere, then dry DMF (10 mL) was added and stirred at 80 °C for 3 h. After that, a 3 mL DMF solution of 1-bromohexane (0.79 g, 4.8 mmol) was added dropwise to the reaction mixture and stirred at 80 °C for another 6 h. The completion of the reaction was monitored with TLC. Then, the reaction mixture was concentrated in vacuum, which was further treated with water. Finally, the crude product was extracted with $CHCl_3$ and the organic layer was removed in a rotary evaporator under reduced pressure. The yellowish liquid of the **C_6-BiP** ligand was purified by silica gel column chromatography using a EtOAc/hexane solvent mixture (2 : 1; v/v), which afforded the product in a good yield (0.38 g, 75%).

Synthesis of [(2,6-bis(1-hexyl-1*H*-benzo[*d*]imidazol-2-yl) pyridine)] platinum(II) chloride (Pt-6). K_2PtCl_4 (0.22 g, 0.52 mmol) was added to a DMSO solution (10 mL) of **C_6-BiP** (0.75 g, 1.56 mmol). The reaction mixture was heated at 90 °C for 10 h. After the reaction, **Pt-6** was precipitated from the crude mixture by adding distilled water. The pure complex was obtained after recrystallization from diethyl ether diffusion in methanol, which yielded 0.38 g of a yellow crystalline solid (yield: 97%).

All the reaction schemes for the ligand and complex are shown in the ESI.†

Oxidase-mimicking activity induced by visible light

The catalytic oxidation of TMB, ABTS, and OPD was used to study the **NanoPtA** oxidase-mimicking activity induced by visible light. In a typical experiment, stock solutions of the catalyst **NanoPtA** (1.0 mM) in methanol and 5.0 mM chromogenic substrates such as TMB, OPD, or ABTS in DMSO were prepared. Catalytic oxidation studies were then performed under visible light where the final solution contained 10 μL of **NanoPtA**, 100 μL of chromogenic substrate and 890 μL of sodium acetate buffer (100 mM, pH 4.0). The reaction solution was irradiated for 10 min with visible light (470 nm) at room temperature and the absorbance maximum was monitored at 652 nm, 418 nm, and 450 nm for TMB, ABTS, and OPD, respectively using a SpectraMax® M5e microplate reader.

Kinetic assay for TMB oxidation

Kinetics studies were carried out with a TMB substrate by varying the concentrations from 0 to 0.5 mM. After 5 min visible light irradiation (470 nm), the colorless solution turned blue. The absorbance was measured at 652 nm. The acquired data were fitted using the Michaelis–Menten equation, and the kinetic parameters were determined.

$$V_0 = \frac{V_{max}[S]}{K_M + [S]}$$

where K_M defines the Michaelis–Menten constant, V_{max} represents the maximum velocity, V_0 is the initial rate, and S represents the substrate concentration.

Detection of ROS and the scavenger study

The ROS generation was measured by using UV-vis absorbance spectroscopy. Various known reactants and scavengers were used to study the presence of ROS. To monitor the presence of singlet oxygen ($^1O_2$), the photooxidation reaction of 1,3-diphenyl isobenzofuran (DPBF) was utilized. A DPBF (20 μM) solution was added to 10 μM **NanoPtA** in 100 mM acetate buffer at (pH 4.0). The solution was kept under visible light irradiation for different intervals of time. The estimation of the singlet oxygen was confirmed in the presence of different scavengers such as sodium azide (10 mM), L-histidine (0.4 mM) as a singlet oxygen quencher, isopropanol as a hydroxyl radical quencher (10 mM), and KI as a H^+ quencher (10 mM), which were added to the vial containing TMB 0.5 mM and 10 μM of **NanoPtA**.

Terephthalic acid (TA) assay

For the TA assay, we used hydrogen peroxide (5.0 mM), terephthalic acid (0.5 mM) and the catalyst **NanoPtA** (10 μM). The assay was performed in 100 mM acetate buffer (pH 4.0). Fluorescence spectra $^{\bullet}OH$ trapped TA was monitored at 435 nm using 315 nm as the excitation wavelength after 1 h irradiation of visible light (470 nm).

Degradation of organic pollutants and neurotransmitter oxidation. The oxidation of organic pollutants was demonstrated using the chromogenic reaction between 1.0 mM of 4-aminoantipyrine (4-AP) and phenolic compounds such as 2,4-dichlorophenol (2,4-DP), phenol, pyrogallol, methoxy phenol and 4-nitrophenol in the concentration range of 0 to 100 μM with 10 μM of **Pt-6** for 10 min irradiation with visible light (470 nm). The colourless solution turned a red colour and the absorbance was measured at 510 nm. For the detection and kinetics studies of the neurotransmitter, a stock solution of 10 mM of dopamine (DA) and adrenaline (AD) was prepared. Using **NanoPtA** (10 μM) and varying concentrations of DA (0–1.0 mM) and AD (0–0.9 mM), respectively in HEPES buffer (10 mM, pH 7.4), the oxidation was examined by the absorbance value at 475 nm for DA and 485 nm for AD after 10 minutes of irradiation visible light (470 nm). LOD was estimated using the method 3σ/slope, where σ is the standard deviation of three blank samples.

Dye degradation. Stock solutions (1.0 mM) of the different dyes, including Trypan blue, Congo red, reactive blue, reactive orange, *etc.*, were prepared in water. We used 10 μM of **NanoPtA** for the degradation of all the dyes under visible light irradiation (470 nm) for 10 min and the different coloured dyes turned colourless. The degradation of dyes was tracked by calculating the absorbance. To determine the stability at different pH values of 4.0, 7.0 and 11.0, we prepared stock solutions of all the dyes at 1.0 mM concentration and 10 μM of **NanoPtA** was taken from 1.0 mM stock, which was irradiated with white light for 10 min.

Reusability. To study the reusability of the system, we used trypan blue dye 10 mM stock solution prepared in water. The catalyst **NanoPtA** (10 μM) was used from 1.0 mM stock in a 2.0 mL vial, 2.0 μL of TrB (20 μM) for each cycle was subsequently added and irradiated with visible light (470 nm) for 10 min. The change in absorbance at 590 nm before and after light irradiation gave us the % of dye degradation.

3. Results and discussion

Fabrication of the self-assembled Pt(II) system

We synthesized three Pt(II) complexes (**Pt-1**, **Pt-6** and **Pt-8**) containing conjugated aromatic tridentate donor ligands substituted with C1, C6 and C8 alkyl chains on the benzimidazole rings (Scheme 1 and Schemes S1 and S2†), with good yields through a slight modification of a previously reported protocol.[44] First, the **BiP** ligand was substituted with an alkyl halide in the presence of a base followed by reaction with K_2PtCl_4 salt to afford the desired **Pt-1**, **Pt-6** and **Pt-8** complexes. The detailed synthetic routes and characterization data are presented in the ESI.† All the ligands and complexes were confirmed by ^1H and ^{13}C NMR spectroscopy and mass spectrometry (Fig. S1–S11†). Next, we studied the self-assembly of **Pt-6** to form **NanoPtA** with increasing water fractions in methanol and investigated its photophysical properties. The decrease of two high energy absorption bands at 310 and 390 nm in the UV-vis spectra of **NanoPtA** (100 μM) are attributed to the intra-ligand charge transfer (ILCT)[44] originating from the n–π* and π–π* transitions (Fig. 1a). A less intense band at 420–500 nm was assigned to the d_{z^2}(Pt)–π* (**C_6-BiP**) metal-to-ligand charge transfer (^{1}MLCT) transition. Notably, a lower energy absorption band at around 550 nm is observed upon introducing water in methanol solution, which is intensified upon increasing the water fraction (Fig. 1a). The plot of absorbance at 550 nm *versus* water volume fraction showed a steady linear increase (Fig. 1b). This band is ascribed to the metal–metal-to-ligand charge transfer (^{1}MMLCT) transition and has been previously described for the formation of Pt···Pt dimers and oligomers.[45]

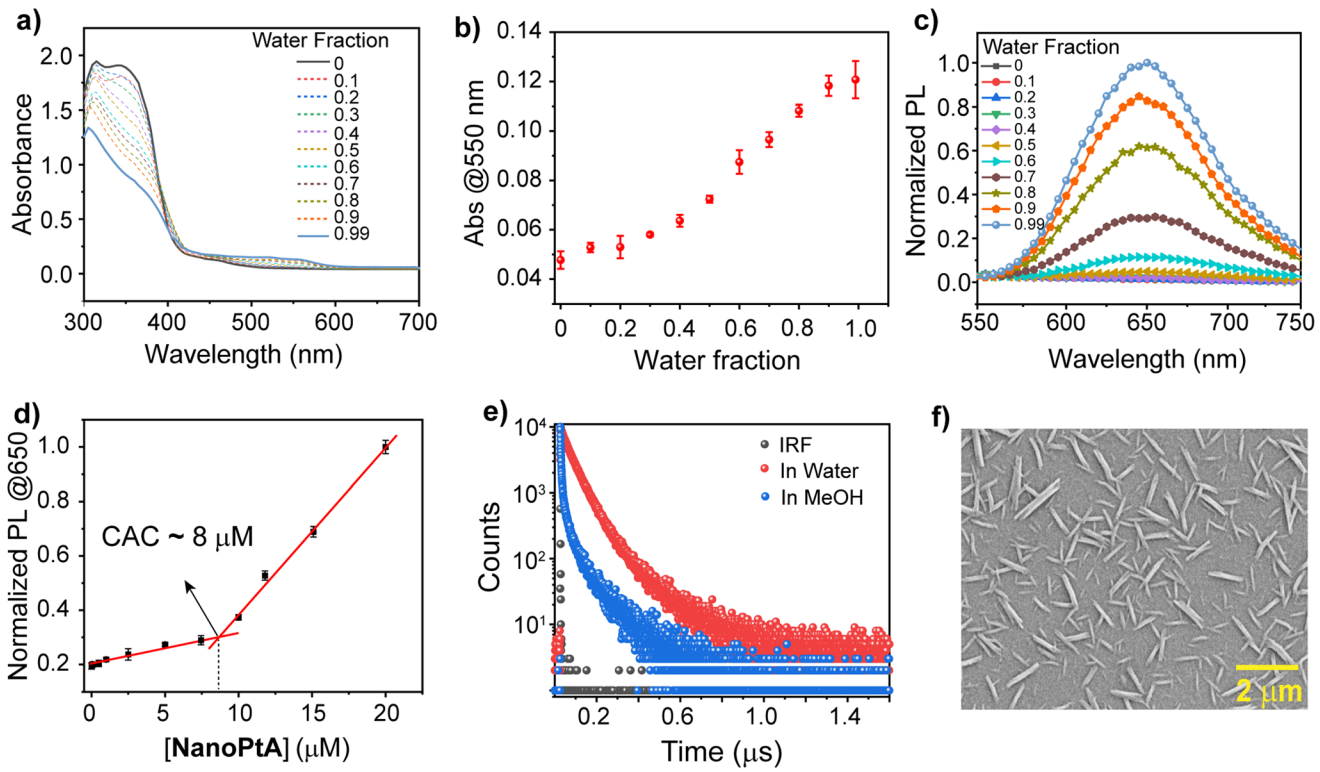

Fig. 1 (a) UV-vis spectra of **NanoPtA** (100 μM) with an increasing volume fraction of water in methanol (0–99%; v/v). (b) Plot of absorbance maxima at 550 nm of **NanoPtA** with increasing water fraction. (c) PL spectra of **NanoPtA** (10 μM) with varying water fractions (0–99%; v/v). (d) Determination of the critical aggregation constant (CAC) of **NanoPtA** by measuring PL intensity at 650 nm. (e) Comparison of the photoluminescence lifetime of **NanoPtA** in MeOH and in aqueous solution, whereas IRF is the instrument response function. (f) FESEM images of the formed assembly of **NanoPtA** in 99% water–methanol.

These results suggest that the **Pt-6** complex tends to undergo self-assembly in water to form **NanoPtA** due to enhanced intermolecular d_{z^2} interactions between the adjacent Pt(II) centres (Pt⋯Pt).[46] Moreover, an aggregation induced emission (AIE) band at 650 nm in the photoluminescence (PL) spectroscopy was observed with an increase in water fraction, which originates from the excited states of the ^{3}MMLCT transition ($\lambda_{exc.}$ 390 nm) (Fig. 1c and S12†) and shows a quantum yield of 12.7% (Fig. S13†). The photophysical properties of the Pt(II) complex were dictated by the aggregation and solubility of the complexes. Notably, **Pt-6** exhibits an enhanced emission and luminescence lifetime in its aggregated state compared to the complexes with lower (**Pt-1**) or higher (**Pt-8**) alkyl chains (Fig. 1e and Fig. S14†). We conducted further studies on **Pt-6** considering these advantageous photophysical properties.

The combined UV-vis and PL spectroscopy results indicate that monomeric **Pt-6** in methanol self-assembles into **NanoPtA** in aqueous medium. Using the self-emissive behaviour of **Pt-6** in higher water fractions, we calculated the critical aggregation constant (CAC) of **NanoPtA** in the 99% water fraction and found the CAC to be as low as ~8 μM (Fig. 1d). Furthermore, the average luminescence lifetime (τ_{av}) of 4.8 ns for **Pt-6** in MeOH increased gradually with the increase in water fraction (40%, 60%, 80%, and 99% water–methanol; v/v) to 137 ns (Fig. 1e and Fig. S15†). This further confirms the existence of ^{3}MMLCT transitions in the aqueous medium, which probably originate from the self-assembled state through noncovalent interactions such as π–π, hydrophobic and Pt⋯Pt interactions between the adjacent centers. In addition, we performed field emission scanning electron microscopy (FESEM) analysis to obtain an insight into the morphology of the self-assembled structures. FESEM images revealed that **NanoPtA** forms nanotape structures with an average length of ~0.5–1.5 μm and width ~90–100 nm (Fig. 1f and Fig. S16†). Besides, dynamic light scattering (DLS) studies revealed that the hydrodynamic diameter of **Pt-6** increased with the increasing polarity of the solvent (Fig. S17†), with the largest diameter ($Z_{average}$) of ~1.1 μM at the highest water fraction (99% water–methanol) (Fig. S17b†). Altogether, we fabricated a tape-like self-assembled structure using aggregation of **Pt-6** in aqueous medium, leading to significant AIE.

Photocatalytic oxidase-like activity of NanoPtA

The emergence of AIE from the self-assembled structure prompted us to explore the oxidase-like activity, which generally depends on ROS. The oxidase-like activity of **NanoPtA** was studied above its CAC (≥8.0 μM) using a colorimetric assay that included substrates 3,3′,5,5′-tetramethylbenzidine (TMB) with an apparent colour change from colourless to blue after oxidation (Fig. 2a).[47] It was observed that the treatment of **NanoPtA** (10 μM) with visible light (at 470 nm) for 10 min turns the TMB (0.5 mM) into a blue coloured solution in acetate buffer (100 mM, pH 4.0) (Fig. 2b). The significant absorbance appearance at 652 nm indicates the oxidation of TMB in the presence of the **NanoPtA** catalyst upon irradiation with visible light. In contrast, TMB did not show any colour change in the absence of the **NanoPtA** catalyst although the reaction mixture was exposed to visible light. To establish the optimum time span for the complete oxidation of TMB, we studied a time dependent TMB absorbance change by varying the light exposure time in the presence of **NanoPtA**. The gradual increase in absorbance at 652 nm with different time intervals (Fig. S18†) confirmed a nearly linear increase in oxidase activity with increasing exposure time, before the saturation at 10 min (Fig. 2c). Further, control experiments with the assembly components such as **C_6-BiP** ligand and K_2PtCl_4 salt even at 5 and 10 equivalents to **NanoPtA**, respectively, did not show significant oxidase activity (Fig. 2d). In fact, the monomeric form of **NanoPtA** in MeOH displayed no enzymatic activity (Fig. 2d), indicating that the excellent oxidase-like activity originated from the assembled state. Further, we tested the activity of the three assembled materials, which showed the most efficient oxidase activity by self-assembled **Pt-6** (Fig. S19†), followed by **Pt-8** and **Pt-1**.

To evaluate the catalytic performance of the **NanoPtA** assembly, we performed steady state kinetic assays with increasing concentrations of TMB in the presence of **NanoPtA** in acetate buffer (100 mM, pH 4.0). Enhanced activity was observed with increasing TMB concentration, which was fitted to the Michaelis–Menten equation. Based on the kinetics plot Fig. 2e, the Michaelis constant (K_M) and the maximal reaction velocity (V_{max}) were determined to be 0.03 mM and 0.105 μM s^{-1}, respectively. The calculated K_M was lower than the previously reported nanozymes, including CeO_2 NPs, and Fe–N/C (Table S1†), indicating that **NanoPtA** possesses a good affinity for TMB. Further, we investigated the practical applicability of **NanoPtA** for the photooxidation of TMB using sunlight. At first, we measured the extent of TMB oxidation by varying both TMB (0–0.5 mM) and **NanoPtA** catalyst concentration (0–50 μM) keeping the same experimental conditions under 10 min sunlight exposure. The results depicted in Fig. S20a† indicate that an increase in the concentration of **NanoPtA** leads to an enhanced yield of oxidized TMB. Also, a substrate concentration-dependent catalytic reaction was observed using a constant catalyst concentration under sunlight (Fig. S20b†). In addition, other substrates like OPD and ABTS were employed to investigate the generalizability of the photocatalytic oxidase-mimicking activity of **NanoPtA** under visible light (470 nm) irradiation. The production of distinct yellow and green colours with absorption maxima at 417 nm and 448 nm,[48] respectively, indicates that **NanoPtA** can oxidize both OPD and ABTS (Fig. S21†). Therefore, it can be confirmed that **NanoPtA** possesses photocatalytic oxidase-mimicking activity for a variety of substrates.

Mechanistic studies of the oxidase-like activity of NanoPtA

Fluorophores that contain benzodiazole, benzothiadiazole, benzotriazole, and metal-based luminescent materials are known to efficiently generate ROS upon photoexcitation through a common mechanism,[49] as illustrated in Fig. 3a. We tested if the oxidase-like activity of **NanoPtA** followed a similar mechanism involving ROS. We employed the ROS detection

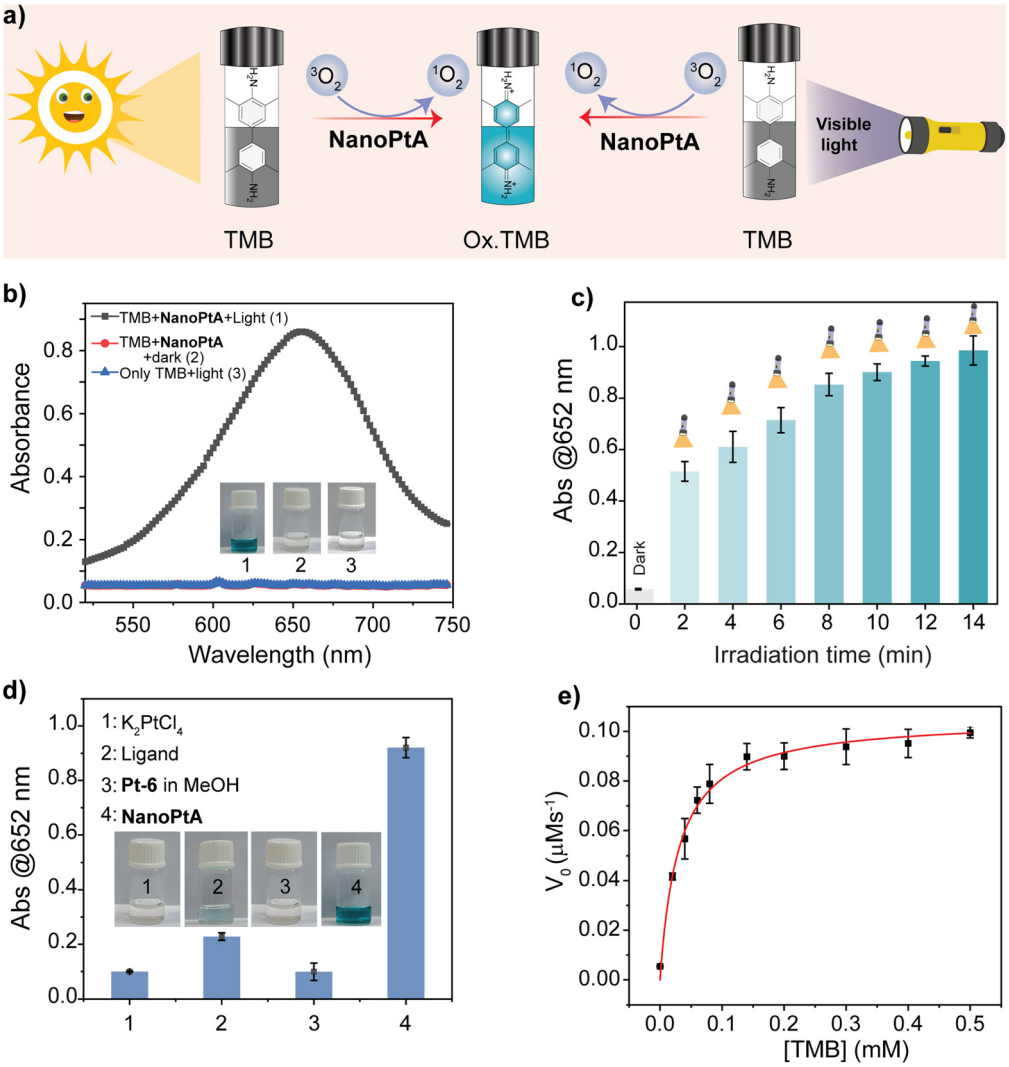

Fig. 2 (a) A schematic representation of TMB oxidation both in the presence of visible light and sunlight. (b) UV-vis spectra of TMB (0.5 mM) in the absence and presence of **NanoPtA** (10 μM) after visible light irradiation (470 nm) in acetate buffer (100 mM, pH 4.0) for 10 min. (c) Absorbance of oxidized TMB (0.5 mM) at 652 nm after visible light irradiation monitored at different time intervals. (d) A comparison of the photo-oxidation of TMB (0.5 mM) by **NanoPtA** (10 μM) in buffer and in methanol and K_2PtCl_4 (100 μM) and the ligand **C_6-BiP** (50 μM) in acetate buffer (100 mM, pH 4.0) for 10 min. (Inset) Images of the corresponding solutions of (1) with K_2PtCl_4, (2) ligand, (3) **Pt-6** in MeOH, and (4) **NanoPtA**. (e) The plot of initial oxidation rate of TMB monitored at 652 nm *versus* TMB concentration (0–0.5 mM) in the presence of **NanoPtA** (10 μM) upon 10 min visible light irradiation. Light source = 470 nm visible light.

agent 1,3-diphenylisobenzofuran (DPBF), which showed an initial light-yellow colour with an absorbance peak at 418 nm. A gradual decrease in the absorption peak was observed with an increasing duration of visible light irradiation (Fig. 3b). This decrease in absorption intensity can be attributed to the photooxidation of DPBF, which resulted in the formation of 1,2-dibenzoyl benzene (DBB) through ring opening,[50] mediated by the singlet oxygen generated (inset of Fig. 3b). However, the DPBF peak did not change in dark conditions even in the presence of **NanoPtA**. These results validate the generation of singlet oxygen as one of the ROS by the **NanoPtA** assembly under visible light irradiation.

Given the common existence of non-specific peroxidase and oxidase-like activities in different nanozymes, we examined the specificity of the self-assembled system. To delineate between the two, we used a terephthalic acid (TA) assay using hydrogen peroxide (H_2O_2). The peroxidase-like activity would decompose H_2O_2 into a highly reactive hydroxyl radical ($^{\bullet}OH$), which reacts with TA to generate 2-hydroxy terephthalic acid (TAOH) (Scheme S3†), resulting in the fluorescence peak at 435 nm (Fig. 3c). The absence of a strong emission band at 435 nm in the presence of **NanoPtA** and H_2O_2 under visible light suggests that the self-assembled system does not produce a hydroxyl radical. Further support of this mechanism was provided by quenching of different reactive species, which may be produced during the aerobic catalytic reaction triggered by visible light. We used quenchers to scavenge different reactive species including $^{\bullet}OH$, $^1O_2$, and photogenerated holes (h^+). The

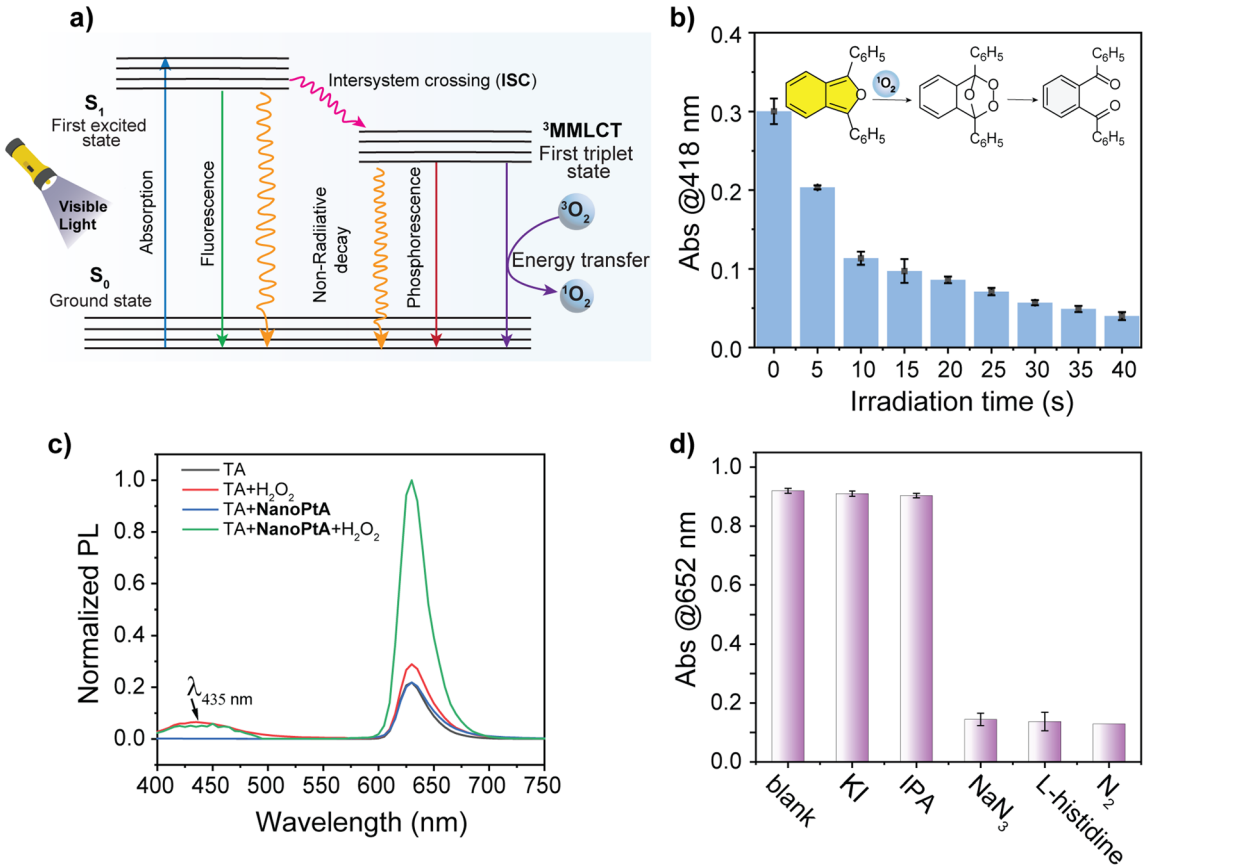

Fig. 3 (a) A schematic representation for the generation of singlet oxygen by **NanoPtA** described by the Jablonski diagram. (b) The extent of photo-oxidation of 1,3-DPBF monitored at 418 nm with variation of illumination time by visible light (470 nm) in the presence of **NanoPtA** (10 μM). (c) The fluorescence spectra of the TA assay for the detection of *in situ* generated hydroxyl radicals (˙OH) using H_2O_2 (5 mM), **NanoPtA** (10 μM) and TA (0.5 mM) after 1 h visible light irradiation. (d) Effects of scavengers on the TMB oxidation in the presence of **NanoPtA** under visible light irradiation. Reaction conditions: 0.5 mM TMB, 10 μM **NanoPtA**, 20 mM IPA, 5 mM KI, 1.0 mM NaN_3, and 0.4 mM L-histidine. Light irradiation time: 10 min.

addition of isopropanol (IPA) as ˙OH scavenger[51] and potassium iodide (KI) as an h^+ scavenger[52,53] did not cause any significant change in the absorbance of the ox.TMB (Fig. 3d), confirming that ˙OH and h^+ were not generated in the catalytic reaction. Conversely, the catalytic activity of **NanoPtA** was significantly suppressed in the presence of NaN_3 and histidine, which were used to scavenge $^1O_2$.[53,54] This suggests that $^1O_2$ is the primary ROS generated in the photocatalytic reaction. Also, the **NanoPtA**-induced catalytic activity was significantly reduced in the absence of dissolved oxygen when the reaction was purged with nitrogen to perform TMB oxidation in an oxygen-free environment. Moreover, according to the Jablonski diagram (Fig. 3a), AIEgen molecules can return to their ground state through three pathways after excitation: (i) fluorescence emission, (ii) generation of reactive oxygen species (ROS) through intersystem crossing (ISC) or transfer to oxygen, and (iii) nonradiative heat dissipation, which are useful for photothermal therapy and photoacoustic imaging.[55] Upon aggregation, **NanoPtA** generates singlet ^{1}MMLCT and triplet ^{3}MMLCT states. Normally, triplet transitions are non-emissive due to the spin selection rule, but the heavy Pt(II) metal center and Pt···Pt interactions in **NanoPtA** allow intersystem crossing, enabling the transition from the singlet to the triplet state by relaxing the spin selection rule. In aqueous solution, dissolved oxygen in the ground state exists in the triplet state. When Pt (II) molecules in the triplet ^{3}MMLCT state interact with oxygen, they transmit their energy to ground state oxygen ($^3O_2$) due to the feasible spin selection rule to produce singlet oxygen ($^1O_2$). Altogether, these studies confirm that the photocatalytic oxidation by **NanoPtA** is exclusively regulated by singlet oxygen, indicating specific oxidase-like activity without any peroxidase-like mechanism.

Photocatalytic oxidation of phenolic pollutants and neurotransmitters

Toxic phenolic aromatics are commonly found in wastewater and effluents from various industries such as chemicals, petrochemicals, pharmaceuticals, textiles, and steel, which cause significant environmental damage.[56] Due to their toxicity, the oxidation and breakdown of phenolic compounds are critical for achieving environmental sustainability. Use of a photocatalytic system would help to produce a viable green techno-

logy for environmental remediation. We investigated the oxidation of different phenolic compounds using **NanoPtA** as a catalyst, in the presence of a chromogenic substrate 4-aminoantipyrine (4-AP) with visible light irradiation for 10 minutes. The oxidized products of phenolic substrates form a red quinone imine adduct with 4-AP (Fig. 4a) with an absorbance at 510 nm. Initially, we performed the catalytic reaction with different concentrations of **NanoPtA** assembly at a constant substrate concentration (1.0 mM of 2,4-DP and 4-AP each) to investigate the effect of the **NanoPtA**. Upon irradiation of visible light for 10 minutes, the absorption peak at 510 nm corresponding to the quinone imine product increased with an increase in concentration of **NanoPtA** (Fig. 4b). Furthermore, we measured the effect of 2,4-DP concentration on the rate of reaction with **NanoPtA**. It can be observed that the rate of reaction increases linearly as depicted by absorbance at 510 nm (Fig. S22†). Notably, the **NanoPtA** catalyst efficiently oxidizes all the phenolic substrates in the presence of light (Fig. 4c). It was observed that the phenolic compounds with electron-withdrawing functional groups were oxidized slower than those with electron-donating groups.[57] Altogether, our study highlights the promising potential of **NanoPtA** as a photocatalyst for the oxidation of organic pollutants containing phenolic groups.

Given the effective catalytic activity of **NanoPtA** in the oxidation of phenolic compounds, we examined the degradation of biologically relevant molecules such as dopamine (DP) and adrenaline (AD), which contain catechol groups. DP is associated with various neurological disorders, including attention deficit hyperactivity disorder, schizophrenia, and neurodegenerative disorders like Alzheimer's and Parkinson's diseases.[58] AD is a crucial neurotransmitter used in the treatment of several medical conditions such as bronchial asthma, cardiac arrest, allergies, and superficial bleeding.[59] Upon the addition of **NanoPtA**, the previously colourless solutions of AD and DP turned brown, indicating the oxidation of these biomolecules.

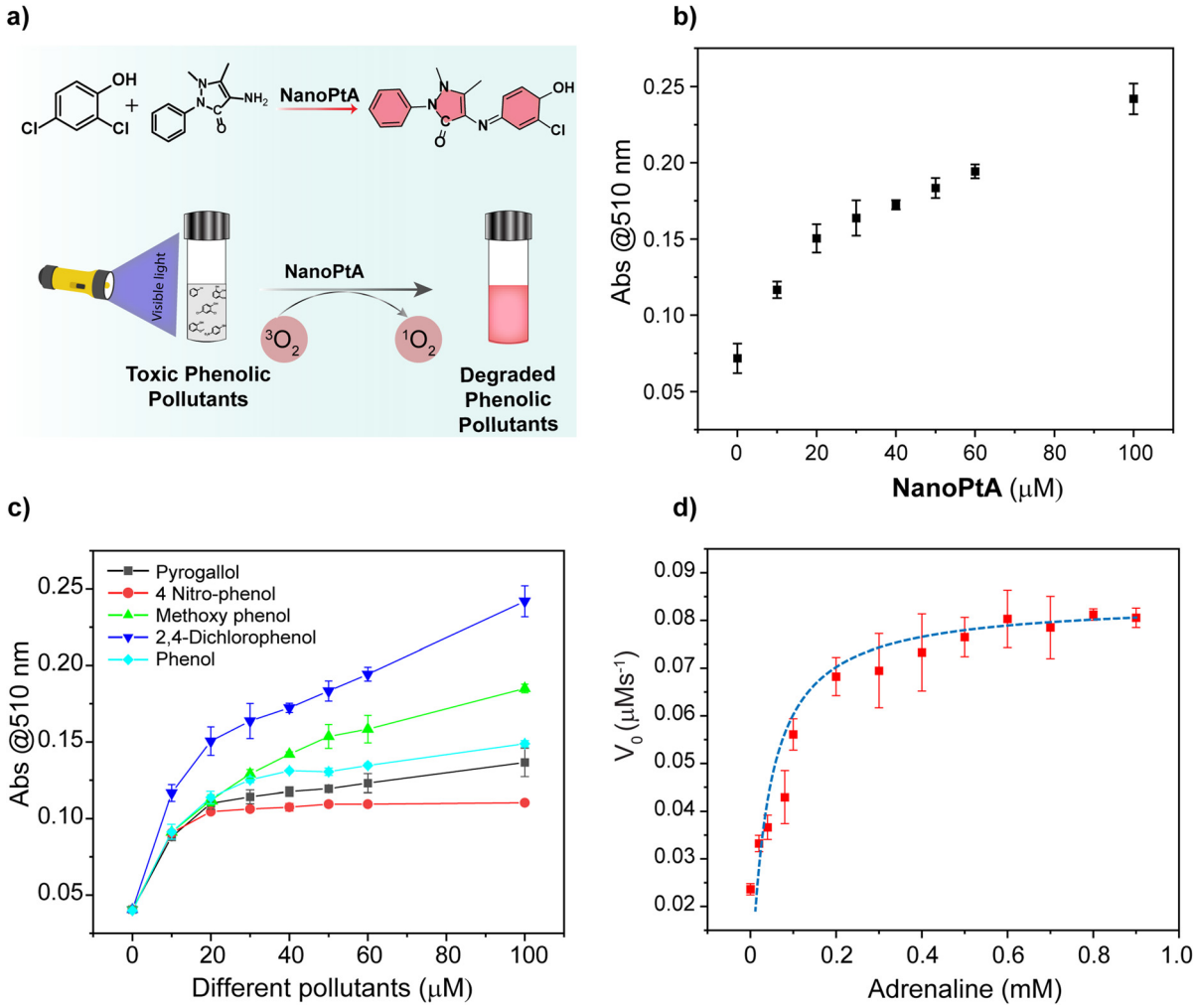

Fig. 4 (a) A schematic representation of the visible light mediated phenolic pollutants degradation by the **NanoPtA** enzyme. (b) UV-vis absorption changes of the chromogenic reaction between 2,4-DP and 4-AP at 510 nm with varying **NanoPtA** concentrations. (c) Oxidation of different phenolic substrates monitored by quinone imine formation at 510 nm catalyzed by **NanoPtA** (10 μM) upon 10 min visible light irradiation. Lines are drawn to guide the eye. (d) A Michaelis–Menten plot of adrenaline oxidation catalyzed by **NanoPtA** (10 μM). Light source: visible light of 470 nm.

To assess the catalytic oxidation of the catecholamines as enzyme substrates, we measured absorbance at 485 nm for AD (Fig. 4d) and 475 nm for DP (Fig. S23†). Interestingly, the oxidation of both AD and DP follow the Michaelis–Menten kinetics, confirming the enzyme-like properties of **NanoPtA**.[6] Given the colorimetric response of the oxidation of the neurotransmitters, this system could be utilized for point-of-care (PoC) detection with a limit of detection (LOD) of 0.7 μM and 4.6 μM for AD and DP, respectively (Fig. S24†). Herein, the LOD was determined from the 3σ/slope of the plots, where σ is the standard deviation of the three blank samples. Also, colorimetric detection of catechol-containing neurotransmitters would enable PoC diagnosis of neurological disorders.

Photocatalytic dye degradation

Organic dyes are a key component of different industries, such as those producing food, leather, textiles, paper, cosmetics, and pharmaceuticals. Even under strict regulations, it has been difficult to restrict the disposal of these dyes into open environments and water bodies, posing a global hazard to human health, aquatic life, and animals.[60] We investigated the capability of **NanoPtA** for dye degradation using the photocatalytic singlet oxygen generation. A 10 min irradiation of Trypan blue (TrB) with visible light (at 470 nm) resulted in immediate decolorization, indicating degradation of the dye. Although 5 μM dye was degraded nearly 100% quantitatively, the 40 μM solution degraded ~95% within this time (Fig. 5a).

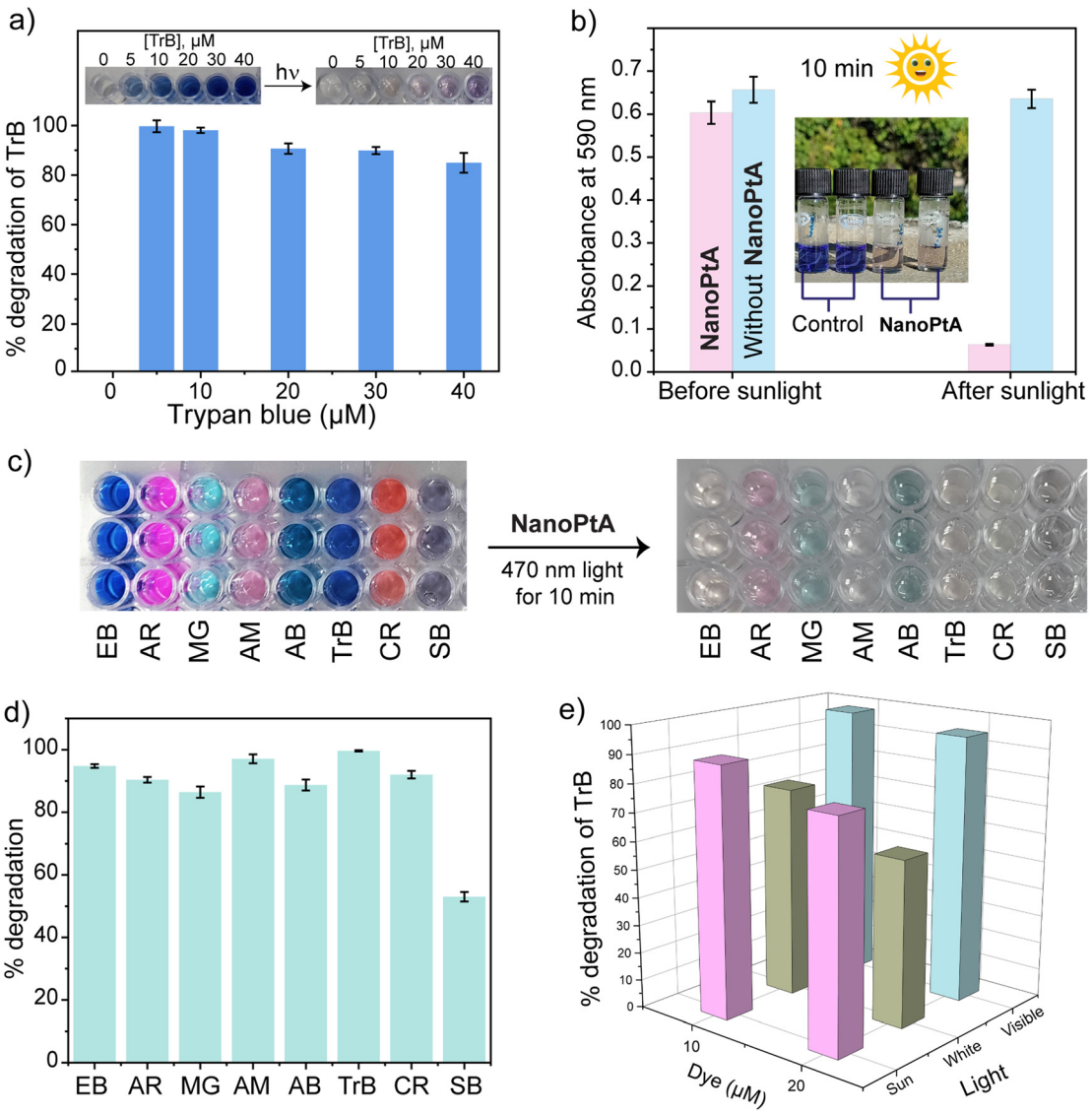

Fig. 5 (a) % of TrB degradation monitored by its absorbance at 590 nm with varying concentrations of TrB dye (0–40 μM). (b) The degradation plot of TrB dye at 550 nm in the presence of **NanoPtA** (10 μM) after 5 min sunlight exposure. (c) Photos of the degradation of different dyes in the presence of **NanoPtA** (10 μM) under visible light. (d) % Degradation plot of multiple dyes with **NanoPtA** (10 μM) under visible light. (e) Comparison of % degradation of TrB dye under exposure of different wavelengths. Light source = visible light 470 nm, white light = 40 W LED bulb.

The control experiment without **NanoPtA** did not cause any decolorization and degradation. Moreover, almost no change was observed for the reaction in the dark with various TrB dye concentrations, indicating that the catalytic dye degradation is photo activated. Further, we tested TrB degradation using sunlight as the excitation source, which would provide a better sustainable solution. A 20 μM TrB solution in water faded within 10 min under sunlight in the presence of 10 μM of **NanoPtA** (Fig. 5b). The absorbance at 590 nm corresponding to the dye showed that ~95% had degraded in 10 min, indicating the high efficiency of the supramolecular nanozyme. However, the dye without **NanoPtA** was not degraded even after shining light for the same duration, demonstrating the nanozyme mediated degradation of the dye.

To further examine the generalizability of **NanoPtA** on more organic azo containing dyes, the photocatalytic degradation of Evans blue (EB), acid red (AR), malachite green (MG), amaranth (AM), amido black (AB), Congo red (CR), and Sudan black (SB) were investigated. The color of the dyes faded rapidly in the presence of **NanoPtA** following visible light irradiation for 10 min (Fig. 5c). In this time, most of the dyes degraded more than 85% up to 98% (Fig. 5d), whereas SB was the least efficient with ~50% degradation. As well as studying dye degradation under sunlight, we also compared the efficiency of three different types of light sources: visible light (470 nm), white light (40-W LED bulb) and sunlight. The dye degradation was efficient under all the sources with 98% under visible light, 89% under sunlight and 75% under white light for a 10 μM dye solution (Fig. 5e). Moreover, **NanoPtA** concentration-dependent dye degradation was noted for all the light conditions (Fig. S25†). Additionally, to confirm the unique oxidase-like activity of **NanoPtA**, we performed a control experiment with H_2O_2 for the degradation of TrB dye in the absence of light with or without **NanoPtA**. As shown in Fig. S26a–S26d,† H_2O_2 was unable to oxidize the TrB dye in the absence of light or **NanoPtA** in the dark, indicating $^1O_2$ mediated dye degradation. Further, we tested if **NanoPtA** exhibits a catalase enzyme-like activity that converts H_2O_2 into H_2O and O_2.[61] A

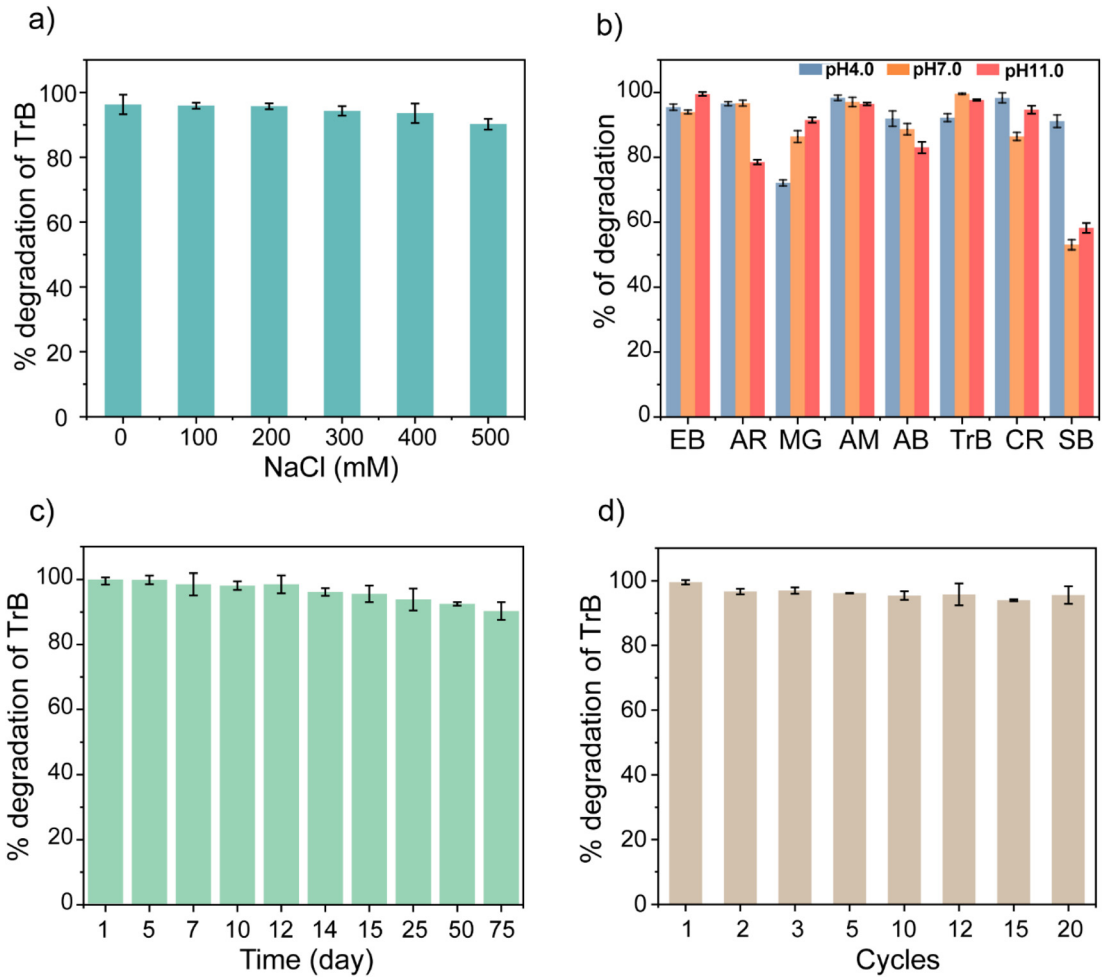

Fig. 6 (a) Effect of NaCl salt concentration on degradation of TrB dye by **NanoPtA**. (b) Comparison of % degradation of different dyes with **NanoPtA** (10 μM) at variable pH values (4.0, 7.0 and 11.0). (c) The % degradation plot of TrB dye, showing the long-term storage catalytic activity of **NanoPtA**. (d) The % degradation plot of TrB dye, relative activity of **NanoPtA** after multiple cycles. Experimental conditions: [TrB] = 20 μM, **NanoPtA** = 10 μM, light source = visible light 470 nm.

reaction mixture containing TrB, H_2O_2 and **NanoPtA** was degassed with N_2 for 10 min to remove the dissolved oxygen, followed by irradiation with 470 nm light for another 10 min. The reaction mixture showed nearly the same absorbance at 590 nm as the control of TrB and **NanoPtA** without H_2O_2 (Fig. S27†). These findings showcase the potential of **NanoPtA** as a specific oxidase-nanozyme in developing sustainable solutions for the degradation of harmful azo dyes in industrial wastewater.

Robustness and reusability of NanoPtA

To make enzyme mimetics practically useful, they need to be robust and stable for longer durations. We studied the stability of the **NanoPtA** assembly by subjecting samples to harsh conditions such as extreme pH, high salt concentration and high temperature. The photocatalytic activity of **NanoPtA** was investigated under different ionic strengths varying the NaCl concentrations from 0 to 500 mM. In our earlier studies, we showed a significant decrease in the inherent activity of the natural oxidases such as laccase with an increase in NaCl concentration.[34] The decline in activity is mainly due to the salting-out effect, which results in the modulation of the enzyme's active site structure and charge distribution.[62] In contrast, the **NanoPtA** assembly exhibited notable effectiveness in a high salinity environment. At least 90% of activity was found to be retained even at a salt concentration of 500 mM (Fig. 6a). This implies that **NanoPtA** is a robust oxidase enzyme-equivalent with potential in practical applications, particularly in treating industrial wastewater, where natural enzymes face difficulties due to the high ionic strength.[62] Furthermore, we studied the photocatalytic activity of the **NanoPtA** assembly at varying pH values (4.0, 7.0, and 11.0) in the presence of visible light by observing the degradation of several dyes (Fig. 6b). It is evident that **NanoPtA** maintained its activity and degraded almost all the dyes by more than 70% except for the SB dye. The SB dye, which lacked *ortho*-hydroxy groups like the other dyes might have caused less degradation. Also, the degradation activity is largely independent of the pH. Moreover, we evaluated the thermostability of **NanoPtA** in solution by measuring its catalytic activity at different temperatures. Fig. S28† shows that **NanoPtA** displayed significant catalytic activity in the temperature range 25–80 °C, retaining at least 85% activity even at 80 °C. In contrast, natural oxidase enzymes such as laccase perform optimally at 50 °C, rapidly losing their activities to only 5% at 80 °C.[63]

Further, the storage stability of **NanoPtA** was investigated at room temperature. It is noteworthy that **NanoPtA** retained >90% of its initial catalytic activity even after 75 days of storage, which was observed from the TrB dye degradation (Fig. 6c). This greater catalytic stability can be attributed to the superior structural stability of the self-assembled system compared to the native enzyme. In general, the self-assembled structure has exceptional operational stability in harsh environments, which enhances its usefulness in real-world applications. Moreover, we evaluated the reusability of **NanoPtA** in the photocatalytic dye degradation. The process involved the degradation of TrB dye by monitoring the absorbance of the system before and after exposing it to visible light in the presence of **NanoPtA**. Additional amounts of dye was added to the same system after complete conversion under light irradiation. It is evident that >98% activity is retained up to the 20th cycle of the catalytic reaction, signifying the robustness of the nanozyme (Fig. 6d). These findings validate the utility of **NanoPtA** for effective environmental remediation in industrial settings.

4. Conclusions

In this work, we introduced a specific enzyme-mimetic activity using a Pt(II)-based supramolecular assembly. While the Pt(II) complex exists as a monomer in methanol, hydrophobic collapse in water leads to aggregated nanotape structures that exhibit AIE. A high luminescence intensity was observed compared to the monomer, leading to the activation of singlet oxygen species upon exposure to visible light. The singlet oxygen-mediated reaction exhibited excellent oxidase-like activity without any peroxidase component, which is a common property of traditional metal-based nanozymes. Another notable feature of the system is the efficient photocatalytic oxidation of phenolic compounds and various azo dyes. These reactions are shown to be effective under visible light sources including sunlight, with quantitative degradation at significantly shorter irradiation times. To address the practical applicability of the supramolecular enzyme mimetic, we demonstrated reusability of **NanoPtA** for at least 20 cycles. Besides, the notable storage stability at room temperature for more than 75 days and unaltered activity in challenging environmental conditions unlike natural enzymes, makes the system a promising candidate for sustainable wastewater treatment. To the best of our knowledge, **NanoPtA** is an exceptional example of a discrete supramolecular structure in water, which exhibits remarkable specific oxidase-like activity *via* photo-induced oxidation. It is anticipated that the extraordinary photocatalytic capabilities of the self-assembled nanozyme will have applications in numerous disciplines, including switchable platforms, biosensing, therapeutics, and environmental protection.

Conflicts of interest

There are no conflicts of interest to declare.

Acknowledgements

S. R. thanks the SERB (grant no. CRG/2022/009021 and ECR/2018/002555) for financial support. The authors thank the Department of Science and Technology (DST-FIST sanction letter no. SR/FST/PSII009/2010) for the instrumental facility at MRC. R. K. acknowledges CSIR for providing a doctoral fellowship. B. S. is thankful for the IISc post-doctoral fellow-

ship under the IOE scheme. A. K. is grateful to MoE for Prime Minister Research Fellowship for doctoral studies.

References

1 E. L. Bell, W. Finnigan, S. P. France, A. P. Green, M. A. Hayes, L. J. Hepworth, S. L. Lovelock, H. Niikura, S. Osuna, E. Romero, K. S. Ryan, N. J. Turner and S. L. Flitsch, *Nat. Rev. Dis. Primers*, 2021, **1**, 46.
2 Y. Huang, J. Ren and X. Qu, *Chem. Rev.*, 2019, **119**, 4357–4412.
3 R. Zhang, X. Yan and K. Fan, *Acc. Mater. Res.*, 2021, **2**, 534–547.
4 H. Wei and E. Wang, *Chem. Soc. Rev.*, 2013, **42**, 6060–6093.
5 L. Gao, J. Zhuang, L. Nie, J. Zhang, Y. Zhang, N. Gu, T. Wang, J. Feng, D. Yang, S. Perrett and X. Yan, *Nat. Nanotechnol.*, 2007, **2**, 577–583.
6 H. Wei, L. Z. Gao, K. L. Fan, J. W. Liu, J. Y. He, X. G. Qu, S. J. Dong, E. K. Wang and X. Y. Yan, *Nano Today*, 2021, **40**, 101269.
7 C. P. Kurup and M. U. Ahmed, *Biosensors*, 2023, **13**, 461.
8 Y. Ai, Z.-N. Hu, X. Liang, H.-B. Sun, H. Xin and Q. Liang, *Adv. Funct. Mater.*, 2022, **32**, 2110432.
9 Y. Tao, E. Ju, J. Ren and X. Qu, *Adv. Mater.*, 2015, **27**, 1097–1104.
10 P. G. Le and M. I. Kim, *Nanomaterials*, 2021, **11**, 2116.
11 L. He, Y. Li, Q. Wu, D. M. Wang, C. M. Li, C. Z. Huang and Y. F. Li, *ACS Appl. Mater. Interfaces*, 2019, **11**, 29158–29166.
12 W. He, Y. Liu, J. Yuan, J.-J. Yin, X. Wu, X. Hu, K. Zhang, J. Liu, C. Chen, Y. Ji and Y. Guo, *Biomaterials*, 2011, **32**, 1139–1147.
13 N. Singh, S. K. NaveenKumar, M. Geethika and G. Mugesh, *Angew. Chem., Int. Ed.*, 2021, **60**, 3121–3130.
14 R. Ragg, A. M. Schilmann, K. Korschelt, C. Wieseotte, M. Kluenker, M. Viel, L. Völker, S. Preiß, J. Herzberger, H. Frey, K. Heinze, P. Blümler, M. N. Tahir, F. Natalio and W. Tremel, *J. Mater. Chem. B*, 2016, **4**, 7423–7428.
15 J. Chen, L. Huang, Q. Wang, W. Wu, H. Zhang, Y. Fang and S. Dong, *Nanoscale*, 2019, **11**, 5960–5966.
16 E. Ghanem and F. M. Raushel, *Toxicol. Appl. Pharmacol.*, 2005, **207**, 459–470.
17 S. Jain, B. Sharma, N. Thakur, S. Mishra and T. K. Sarma, *ACS Appl. Nano Mater.*, 2020, **3**, 7917–7929.
18 J. Chen, Q. Ma, M. Li, D. Chao, L. Huang, W. Wu, Y. Fang and S. Dong, *Nat. Commun.*, 2021, **12**, 3375.
19 C. Wang, Y. Li, W. Yang, L. Zhou and S. Wei, *Adv. Healthcare Mater.*, 2021, **10**, 2100601.
20 C.-P. Liu, T.-H. Wu, C.-Y. Liu, K.-C. Chen, Y.-X. Chen, G.-S. Chen and S.-Y. Lin, *Small*, 2017, **13**, 1700278.
21 G. J. Colpas, B. J. Hamstra, J. W. Kampf and V. L. Pecoraro, *J. Am. Chem. Soc.*, 1996, **118**, 3469–3478.
22 M. Hu, K. Korschelt, M. Viel, N. Wiesmann, M. Kappl, J. Brieger, K. Landfester, H. Thérien-Aubin and W. Tremel, *ACS Appl. Mater. Interfaces*, 2018, **10**, 44722–44730.
23 W. Chen, S. Li, J. Wang, K. Sun and Y. Si, *Nanoscale*, 2019, **11**, 15783–15793.
24 N. Alizadeh and A. Salimi, *J. Nanobiotechnol.*, 2021, **19**, 26.
25 Z. Wang, R. Zhang, X. Yan and K. Fan, *Mater. Today*, 2020, **41**, 81–119.
26 R. Huang, C.-H. Li, R. Cao-Milán, L. D. He, J. M. Makabenta, X. Zhang, E. Yu and V. M. Rotello, *J. Am. Chem. Soc.*, 2020, **142**, 10723–10729.
27 D. Velasco, E. Tumarkin and E. Kumacheva, *Small*, 2012, **8**, 1633–1642.
28 M. Li, J. Chen, W. Wu, Y. Fang and S. Dong, *J. Am. Chem. Soc.*, 2020, **142**, 15569–15574.
29 H. Cheng, Y. Liu, Y. Hu, Y. Ding, S. Lin, W. Cao, Q. Wang, J. Wu, F. Muhammad, X. Zhao, D. Zhao, Z. Li, H. Xing and H. Wei, *Anal. Chem.*, 2017, **89**, 11552–11559.
30 J. S. Siegel, *Science*, 1996, **271**, 949–949.
31 Z. Dong, W. Yongguo, Y. Yin and J. Liu, *Curr. Opin. Colloid Interface Sci.*, 2011, **16**, 451–458.
32 M. D. Toscano, K. J. Woycechowsky and D. Hilvert, *Angew. Chem., Int. Ed.*, 2007, **46**, 3212–3236.
33 X. Huang, Z. Dong, J. Liu, S. Mao, J. Xu, G. Luo and J. Shen, *Langmuir*, 2007, **23**, 1518–1522.
34 M. Solra, S. Das, A. Srivastava, B. Sen and S. Rana, *ACS Appl. Mater. Interfaces*, 2022, **14**, 45096–45109.
35 M. O. Guler and S. I. Stupp, *J. Am. Chem. Soc.*, 2007, **129**, 12082–12083.
36 Y. Tang, L. Zhou, J. Li, Q. Luo, X. Huang, P. Wu, Y. Wang, J. Xu, J. Shen and J. Liu, *Angew. Chem., Int. Ed.*, 2010, **49**, 3920–3924.
37 P. Bhatt, M. Solra, S. I. Chaudhury and S. Rana, *Biosensors*, 2023, **13**, 277.
38 Y. Gao, F. Zhao, Q. Wang, Y. Zhang and B. Xu, *Chem. Soc. Rev.*, 2010, **39**, 3425–3433.
39 J. Mei, N. L. C. Leung, R. T. K. Kwok, J. W. Y. Lam and B. Z. Tang, *Chem. Rev.*, 2015, **115**, 11718–11940.
40 X. Lin, F. Chen, X. Yu, H. Wang, H. Qiu, Y. Li, S. Yin and P. J. Stang, *Proc. Natl. Acad. Sci. U. S. A.*, 2022, **119**, e2203994119.
41 A. J. McConnell, *Chem. Soc. Rev.*, 2022, **51**, 2957–2971.
42 H. Rao, X. Xue, M. Luo, H. Liu and Z. Xue, *Chin. Chem. Lett.*, 2021, **32**, 25–32.
43 X. Zheng, M. H.-Y. Chan, A. K.-W. Chan, S. Cao, M. Ng, F. K. Sheong, C. Li, E. C. Goonetilleke, W. W. Y. Lam, T.-C. Lau, X. Huang and V. W.-W. Yam, *Proc. Natl. Acad. Sci. U. S. A.*, 2022, **119**, e2116543119.
44 I. Mathew and W. Sun, *Dalton Trans.*, 2010, **39**, 5885–5898.
45 C. Po, A. Y.-Y. Tam, K. M.-C. Wong and V. W.-W. Yam, *J. Am. Chem. Soc.*, 2011, **133**, 12136–12143.
46 Y.-S. Wong, M. Ng, M. C.-L. Yeung and V. W.-W. Yam, *J. Am. Chem. Soc.*, 2021, **143**, 973–982.
47 L. A. Marquez and H. B. Dunford, *Biochemistry*, 1997, **36**, 9349–9355.
48 L. Liu, C. Sun, J. Yang, Y. Shi, Y. Long and H. Zheng, *Chem. – Eur. J.*, 2018, **24**, 6148–6154.
49 M. C. DeRosa and R. J. Crutchley, *Coord. Chem. Rev.*, 2002, **233–234**, 351–371.

50 P. P. Neelakandan, A. Jiménez, J. D. Thoburn and J. R. Nitschke, *Angew. Chem., Int. Ed.*, 2015, **54**, 14378–14382.
51 C. An, J. Wang, C. Qin, W. Jiang, S. Wang, Y. Li and Q. Zhang, *J. Mater. Chem.*, 2012, **22**, 13153–13158.
52 R. Ma, X. Wang, J. Huang, J. Song, J. Zhang and X. Wang, *Vacuum*, 2017, **141**, 157–165.
53 M. Bancirova, *Luminescence*, 2011, **26**, 685–688.
54 I. B. C. Matheson, R. D. Etheridge, N. R. Kratowich and J. Lee, *Photochem. Photobiol.*, 1975, **21**, 165–171.
55 G. X. Feng, G. Q. Zhang and D. Ding, *Chem. Soc. Rev.*, 2020, **49**, 8179–8234.
56 S. Zhang, F. Lin, Q. Yuan, J. Liu, Y. Li and H. Liang, *J. Environ. Sci.*, 2020, **88**, 103–111.
57 X. Xu, J. Wang, R. Huang, W. Qi, R. Su and Z. He, *Catal. Sci. Technol.*, 2021, **11**, 3402–3410.
58 H. Juárez Olguín, D. Calderón Guzmán, E. Hernández García and G. Barragán Mejía, *Oxid. Med. Cell. Longevity*, 2016, **2016**, 9730467.
59 K. S. R. Sastry, Y. Karpova, S. Prokopovich, A. J. Smith, B. Essau, A. Gersappe, J. P. Carson, M. J. Weber, T. C. Register, Y. Q. Chen, R. B. Penn and G. Kulik, *J. Biol. Chem.*, 2007, **282**, 14094–14100.
60 D. Ayodhya and G. Veerabhadram, *Mater. Today Energy*, 2018, **9**, 83–113.
61 P. Campomanes, U. Rothlisberger, M. Alfonso-Prieto and C. Rovira, *J. Am. Chem. Soc.*, 2015, **137**, 11170–11178.
62 A. M. Hyde, S. L. Zultanski, J. H. Waldman, Y.-L. Zhong, M. Shevlin and F. Peng, *Org. Process Res. Dev.*, 2017, **21**, 1355–1370.
63 T. Maity, S. Jain, M. Solra, S. Barman and S. Rana, *ACS Sustainable Chem. Eng.*, 2022, **10**, 1398–1407.